RSC Advances

PAPER

View Article Online
View Journal | View Issue

Cite this: *RSC Adv.*, 2022, **12**, 19495

Engineering exposed vertical nano-TiO_2 (001) facets/BiOI nanosheet heterojunction film for constructing a satisfactory PEC glucose oxidase biosensor†

Baiqiang Wu,[a] Zike Cheng,[a] Yao Hou,[a] Qian Chen,*[b] Xiaohong Wang,[a] Bin Qiao,[c] Delun Chen[a] and Jinchun Tu *[a]

In the field of photoelectrochemical (PEC) enzyme biosensors, constructing efficient photoelectrodes, in which the recombination of photogenerated carriers is an important factor affecting the performance, is of great significance. Herein, to enhance the separation efficiency of photogenerated carriers, titanium dioxide (TiO_2) nanosheet (NS)/bismuth oxyiodide (BiOI) NS/glucose oxidase (GOx) composites were prepared *via* hydrothermal and solvothermal methods. Single-crystal anatase TiO_2 NSs with a high percentage of (001) facets lead to better photocarrier separation due to heterojunctions between facets. After coupling with BiOI NSs, the photoelectrochemical performance of the electrode was greatly improved. The photogenerated electrons from TiO_2 and BiOI gathered at TiO_2 (101) and were exported through the fluorine-doped tin oxide (FTO) substrate to generate electrical signals. Photogenerated holes were transferred to TiO_2 (001) and BiOI to participate in the enzymatic reaction, showing the outstanding separation of electrons and holes. The prepared TiO_2 NS/BiOI NS/GOx glucose biosensor achieved satisfactory results, with sensitivity of 14.25 μA mM^{-1} cm^{-2}, a linear measurement range of 0–1 mM, and a limit of detection (3S/N) of 0.01 mM in phosphate buffered saline (PBS) at a pH of 7.4. The mechanism for the efficient separation of photogenerated carriers based on the facet heterojunctions introduced in this paper also provides new insights into other optoelectronic biosensors.

Received 16th May 2022
Accepted 23rd June 2022

DOI: 10.1039/d2ra03070e

rsc.li/rsc-advances

1. Introduction

Photoelectrochemical (PEC) stands out for its advantages of low cost, high sensitivity, and strong anti-interference, and has broad application foregrounded in biological analysis.[1,2] The performance of photoelectrodes plays a crucial role in biosensors, and the recombination of photogenerated carriers in the bulk phase is one of the factors affecting performance. Therefore, constructing an electrode that could efficiently separate photogenerated carriers is important.

Two-dimensional titanium dioxide (TiO_2) nanosheets (NSs) are splendid alternatives for PEC biosensors due to their high specific surface area and chemical reaction facets. Compared with one-dimensional TiO_2 nanorods, anatase TiO_2 NSs with a high percentage of (001) facets are more competitive in solar cells, photonic and optoelectronic devices, sensors, and the photocatalysis field.[3] Previous reports showed that anatase TiO_2 (101) are enriched facets for electrons. The electrons generated by photoexcitation on (001) facets would spontaneously migrate to (101) facets.[4] This behavior could alleviate the problem of bulk recombination of photogenerated carriers for single crystal materials. However, the application of TiO_2 in the visible light range is very restricted due to its large band gap energy.[5] To improve the response of TiO_2 in the visible light range, common methods include deposition of noble metal quantum dots, element doping, and modification with narrow band gap semiconductors.[6–8] Bismuth oxyiodide (BiOI) is a p-type semiconductor that has a narrow band gap between 1.7 and 1.9 eV, and a visible light response.[9] After p-type BiOI has been assembled with n-type TiO_2, the photogenerated electrons of BiOI quickly transfer to the conduction band of TiO_2, and the photogenerated holes of TiO_2 move to the valence band of BiOI, thereby achieving separation of electrons and holes.[10]

[a]*State Key Laboratory of Marine Resource Utilization in South China Sea, College of Materials Science and Engineering, Hainan University, Haikou 570228, China. E-mail: tujinchun@hainanu.edu.cn*

[b]*Department of Clinical Laboratory, The First Affiliated Hospital of Hainan Medical University, Haikou 570102, China. E-mail: 251100736@qq.com*

[c]*Department of Clinical Laboratory of the Second Affiliated Hospital, School of Tropical Medicine, Key Laboratory of Emergency and Trauma of Ministry of Education, Research Unit of Island Emergency Medicine, Chinese Academy of Medical Sciences (No. 2019RU013), Hainan Medical University, Haikou 571199, China*

† Electronic supplementary information (ESI) available. See https://doi.org/10.1039/d2ra03070e

Herein, a PEC enzyme biosensor was developed based on BiOI NS modified TiO_2 NSs for glucose detection. TiO_2 NSs were uniformly grown on the surface of a fluorine-doped tin oxide (FTO) substrate by a hydrothermal method. The tight binding of TiO_2 to the substrate was beneficial to the transport of electrons. Furthermore, the exposed (001) facets of TiO_2 contributed to the separation of photogenerated carriers due to facet heterojunctions. In addition, BiOI NSs grown *in situ* on TiO_2 (101) planes by the solvothermal method could form a heterojunction with TiO_2 and improve the separation of photogenerated charges and the absorption of material in the visible light range. The (101) facet of TiO_2 acted as an electron-rich facet to accept photogenerated electrons from the (001) facets and BiOI, and transported them to the external circuit through the FTO substrate, whereas the photogenerated holes were transferred to the (001) facets and BiOI to participate in the enzymatic reaction, so that the electrons and holes were separated in space. In conclusion, the synergistic effect of crystal-plane heterojunctions and narrow-band gap semiconductors enhances the separation efficiency of photogenerated carriers and the absorption of visible light, providing new insights for other optoelectronic biosensors.

2. Experimental

2.1 Reagents and materials

FTO substrates were acquired from Outhwaite New Energy Company. Ammonium fluorotitanate ($(NH_4)_2TiF_6$), tetrabutyl titanate ($C_{16}H_{36}O_4Ti$), glucose oxidase (GOx), and bismuth nitrate pentahydrate ($Bi(NO_3)_3 \cdot 5H_2O$) were purchased from Shanghai Maclin Biochemical Technology Co., Ltd. Ethylene glycol, ethanol, potassium iodide (KI), glucose, and hydrochloric acid (HCl) were acquired from the Guangzhou Chemical Reagent Factory. The water solvent was ultrapure water prepared in the laboratory. All reagents and solutions were not further processed.

2.2 Synthesis of TiO_2 NSs

The FTO substrates were thoroughly ultrasonically cleaned in isopropyl alcohol, acetone, and water for 20 min, and dried under pure argon flow gas for later use. Concentrated HCl was diluted with ultra-pure water at a ratio of 1 : 1 and stirred for 10 min. Then, 0.4 mL of tetrabutyl titanate was added drop by drop to 20 mL of diluted HCl and stirred vigorously for 30 min. Next, 0.15 g of ammonium fluorotitanate was added to the

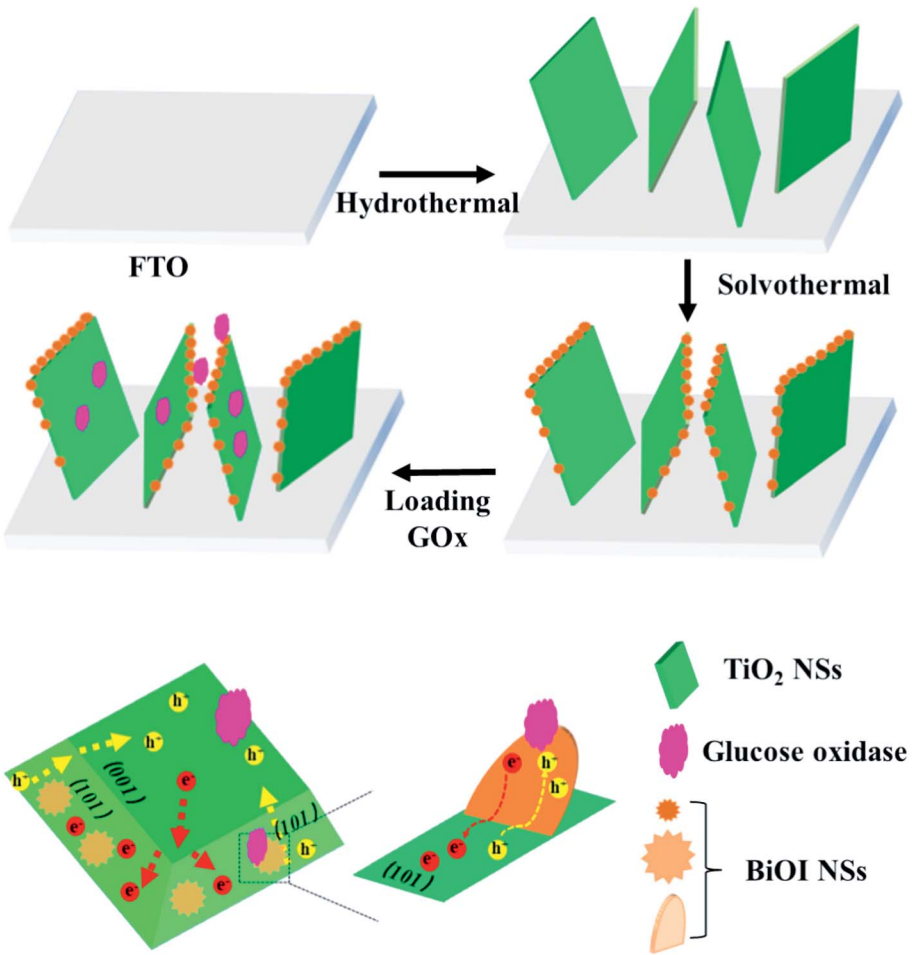

Scheme 1 The fabrication of the TiO_2 NS/BiOI NS electrode.

above solution and stirred for 30 min. Then, the mixture was transferred to a 30 mL inner lining of the autoclave, which contained the prepared FTO substrates. The conductive side of the FTO faced down, and the angle between it and the inner wall of the Teflon-lined autoclave was about 30°. After 12 h of hydrothermal reaction at 170 °C, when the autoclave was completely cooled down naturally, the samples were removed, thoroughly rinsed with deionized water, dried at 60 °C for 2 h in an oven, and annealed at 450 °C for 2 h in air.

2.3 Synthesis of TiO_2 NSs/BiOI NSs

The TiO_2 NS/BiOI NS electrode was synthesized by the secondary solvothermal method. 10 mM of KI and $Bi(NO_3)_2$ ethylene glycol solution were prepared and fully stirred. 10 mL of $Bi(NO_3)_2$ ethylene glycol solution was poured into a beaker, and kept under vigorous stirring; then 10 mL of KI ethylene glycol solution was added into the beaker dropwise, with continuous stirring for 30 min. Next, the resultant solution was transferred to a 30 mL Teflon-lined autoclave, which contained the FTO substrates with TiO_2 NSs. The temperature and time of the solvothermal reaction were set to 160 °C and 10 h, respectively. Finally, the samples were rinsed thoroughly with water and ethanol, and then dried in an oven at 60 °C for 2 h.

2.4 Fabrication of the PEC electrode

The prepared TiO_2 NS/BiOI NS electrodes were placed in a freezer at 4 °C for 30 min. The preparation of the electrode is shown in Scheme 1. Then, 15 μL of activated glucose oxidase 10 mg mL^{-1}, Nafion solvent (1% w/w) solution, and 5 μL of chitosan solution were dropped onto the surface of the electrode and placed in an environment of 4 °C for 48 h until the surface liquid was completely dry.

2.5 Detection and instruments

The electrochemical tests used equipment from Chenhua Electrochemical Equipment, Shanghai, China, and the model was CHI660E. The light source was a simulated daylight xenon light source provided by Beijing CEAuLight Technology Co., Ltd, and the product model was CEL-S500. The X-ray diffraction (XRD) analysis used an instrument from the Rigaku Co., Ltd of Japan. The equipment model was D/max 2550 V, diffracted with monochromatized Cu Kα radiation (λ = 0.15418 nm). In the experimental test, the rotation angle went from 10° to 80°, the scanning speed was 10° min^{-1}, and each step was 0.01°. The UV-visible light absorption spectrum was taken with a Japanese Jasco UV-Vis absorption spectrophotometer; the model was UV-550, and the wavelength range set in this experiment went from

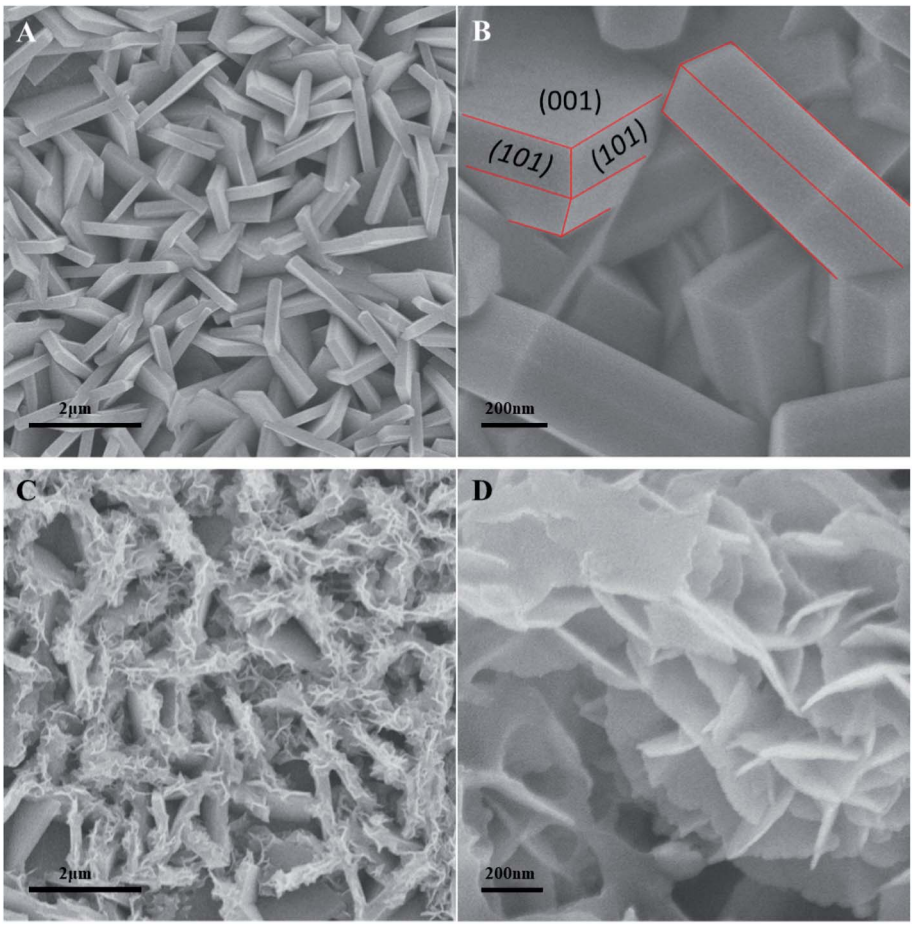

Fig. 1 SEM images of (A and B) TiO_2 NSs and (C and D) TiO_2 NSs/BiOI NSs.

200 nm to 800 nm. The scanning electron microscope (SEM) was supplied by Hitachi, Japan, and the model was Hitachi SU 8010. The transmission electron microscope (TEM) was manufactured by JEOL, Japan, and the model was JEOL JEM 2100. The chemical composition of the sample was measured by an X-ray electron spectroscopy (XPS) instrument produced by Kratos; the model was Axis Ultra DLD, and the excitation source was an Al-Kα monochromator.

3. Results and discussion

To characterize the morphology of the electrode materials, the materials prepared in this work were observed by SEM. Fig. 1A shows that the FTO substrates are densely and uniformly covered with NSs, which cross one another and are closely arranged. The intimate, homogeneous combination between TiO_2 NSs and FTO substrate could ensure fast electron transfer. Fig. S1† shows that MnO_2 is photo-deposited on the TiO_2 NSs. The results show that MnO_2 has the characteristics of selective growth in space, indicating that the exposed facets are hole-enriched (001) facets. Fig. 1B shows that the upper and lower sides of the NSs are square (001) facets, the sides are composed of symmetrical isosceles trapezoids corresponding to the (101) facets, the average thickness of the NS is about 190 nm, and the average side length of the NS is about 1.2 μm.

Fig. 1C and D present the TiO_2 NS/BiOI NS images synthesized by a secondary solvothermal method. A cluster of NS structures grows on top of the TiO_2 NSs. In addition, Fig. 1C shows that BiOI NSs selectively grow on the (101) facets of TiO_2. Combined with the results of XPS, TiO_2 NSs still contain a small amount of F^+ after annealing, which is closely combined with TiO_2 (001) facets as a morphology regulator. The reason could be the repulsion between halogen atoms, which is not conducive to BiOI NS growth on TiO_2 (001) facets. In Fig. 1D, the

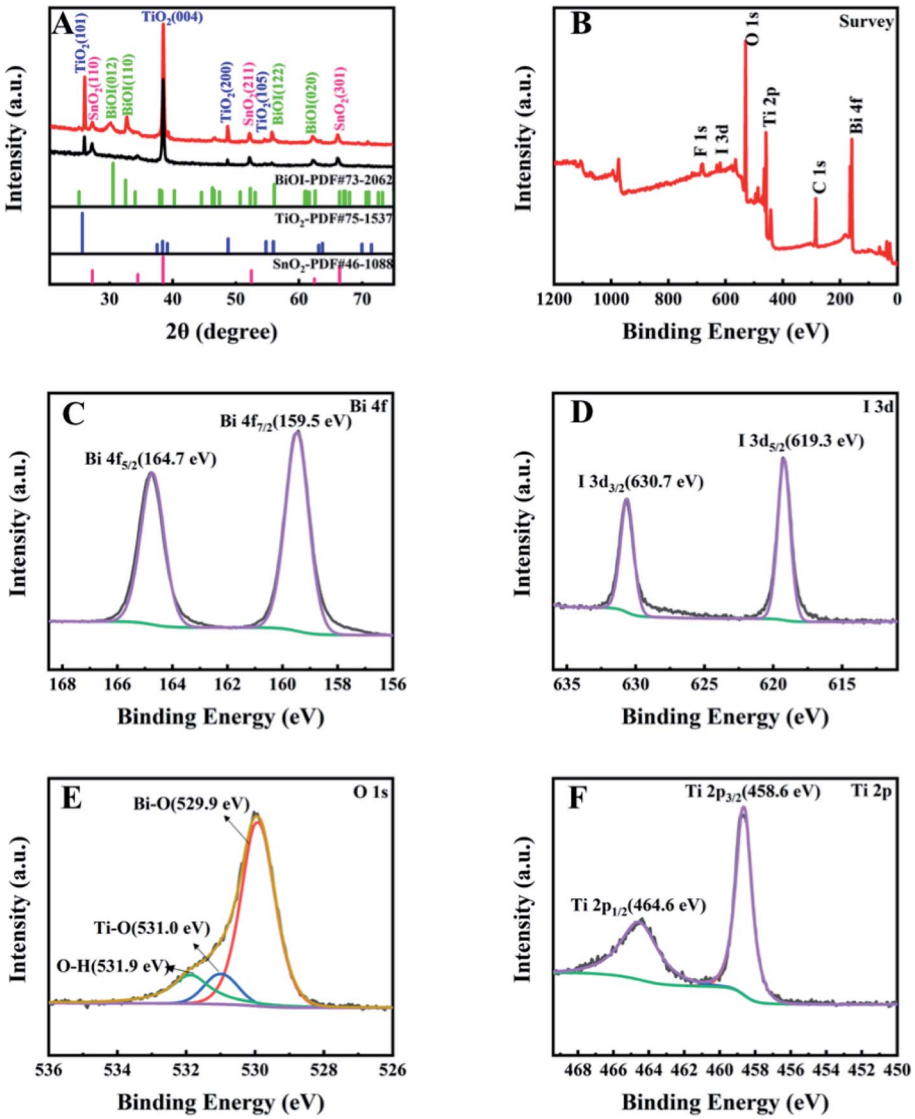

Fig. 2 (A) XRD patterns of TiO_2 NSs (black curve) and TiO_2 NSs/BiOI NSs (red curve). XPS patterns: (B) survey spectra, (C) Bi 4f, (D) I 3d, (E) O 1s, and (F) Ti 2p.

thickness of the BiOI nano structure in the magnified image is about 20 nm.

To investigate the crystal structure of the electrode materials, the materials synthesized in this work were analyzed by XRD. The black and red curves in Fig. 2A are the XRD patterns of TiO_2 NSs and TiO_2 NSs/BiOI NSs, respectively, and the crystal planes of the substances corresponding to the diffraction peaks are marked. The prepared TiO_2 NSs are in the anatase phase. Diffraction peaks located at 25.9°, 38.4°, and 48.6° correspond to the (101), (004), and (200) facets of TiO_2, respectively, consistent with the PDF standard card JCPDS Number 75-1537. The diffraction peaks (red curve) at 29.7°, 31.7°, 45.5°, and 51.4° correspond to the (012), (110), (020), and (114) facets of BiOI, respectively, indicating that the prepared BiOI NSs have a tetragonal chloroformate structure[11] and correspond to the standard PDF card JCPDS Number 73-2062. The diffraction peaks are very sharp, verifying the high crystallinity of the samples. Thus, a binary composite composed of TiO_2 NSs and BiOI NSs was successfully synthesized. XPS was used to explore the elemental composition and valence state of the TiO_2 NS/BiOI NS electrode. According to the survey XPS spectrum of Fig. 2B, the main constituent elements of the electrode are Bi, I, O, and Ti (the spectrum was calibrated with the banding energy of C 1s). The high-resolution spectrum of each element is collated in Fig. 2C–F. Fig. 2C shows two Bi 4f peaks for the sample at 159.5 and 164.7 eV, which are attributed to Bi $4f_{7/2}$ and Bi $4f_{5/2}$, respectively.[12] Fig. 2D shows two I 3d peaks at 619.3 and 630.7 eV that belong to I $3d_{5/2}$ and I $3d_{3/2}$, respectively, meaning that the valence of I is negative monovalent.[13] Fig. 2E shows that the O 1s peaks consist of three individual binding energies of 529.9, 531.0, and 531.9 eV that could belong to the Bi–O bond, Ti–O bond, and O–H bond, respectively.[14,15] In addition, the appearance of an O–H bond may be due to the hydroxyl group in the water adsorbed by the sample.[16] Fig. 2F shows that the two peaks at 458.6 and 464.6 eV are assigned to Ti $2p_{3/2}$ and Ti $2p_{1/2}$, indicating that the valence of Ti is +4.[17]

The microstructure and morphology of TiO_2 NSs and TiO_2 NSs/BiOI NSs were further characterized by TEM. Fig. 3A shows the TEM image of the prepared TiO_2 NSs. The morphology is matched with that observed by SEM, showing a rectangular outline. Fig. 3B shows the crystalline lattice fringes of TiO_2 NSs in the enlarged image are 0.35 nm, which correspond to anatase (101) facets. The selected area electron diffraction (SAED) pattern is taken from the NS part, according to the bright, periodically arranged diffraction spots, indicating that the prepared TiO_2 NSs are single crystals and show excellent

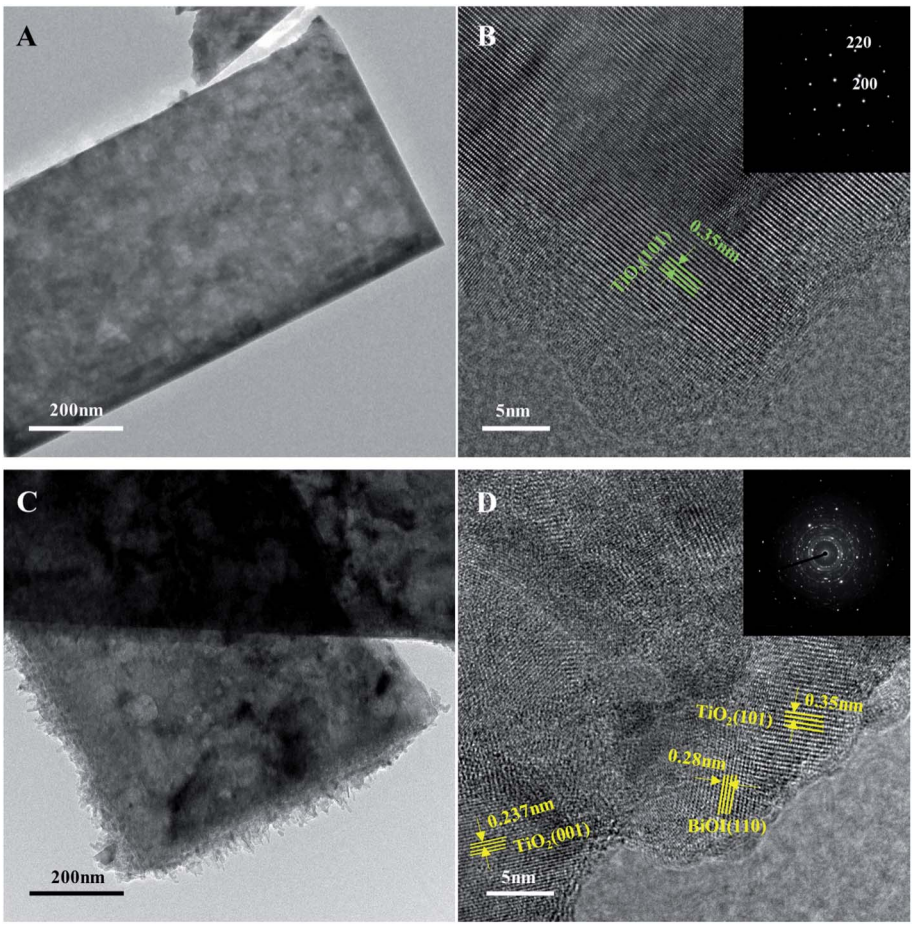

Fig. 3 (A) TEM and (B) HRTEM images of TiO_2 NSs and (inset) the SAED pattern. (C) TEM and (D) HRTEM images of TiO_2 NSs/BiOI NSs and (inset) the SAED pattern.

crystallinity.[18] The distance between the diffraction spots and the center point was measured and proofread with standard PDF cards, suggesting that the TiO_2 NSs are taken along the [001] zone axis.[19] Fig. 3C is the TEM image of a single TiO_2 NS grown with BiOI NSs. Nanosized lamellar structures selectively grow on the edge of the NS, and the results are consistent with the SEM observations. Fig. 3D is a high-resolution TEM image showing the clear lattice fringes of the TiO_2 NS/BiOI NS structure. The lattice spacings of 0.237 and 0.35 nm correspond to the (001) and (101) facets of anatase phase TiO_2, respectively. In addition, the lattice fringes exhibit a lattice spacing of 0.28 nm, corresponding to the (110) facets of BiOI. The inset SAED of the area of Fig. 3D shows a ring-like pattern and has a polycrystalline feature. The EDS spectra and EDX mapping images (Fig. S2†) of the TiO_2 NSs/BiOI NSs further confirm the successful preparation of TiO_2 and BiOI binary composite electrodes.

The light absorption properties of TiO_2 NSs and TiO_2 NSs/BiOI NSs in the range of 250–800 nm were studied with UV-vis diffuse reflectance spectra. Fig. 4A shows that, after BiOI NSs were modified on TiO_2 NSs, the absorption peaks of the samples shifted significantly to the visible region, and the absorption edge increased from 391 nm to 544 nm because BiOI is a narrow band gap semiconductor and could be excited by longer wavelength light, which is beneficial to keeping the bioactivity of the enzyme immobilized on the TiO_2 NS/BiOI NS electrode[11] and reducing the occurrence of side reactions in the detection system.[20]

The band gap values could be calculated with the following formula:[21]

$$(\alpha h\nu)^n = B(h\nu - E_g) \quad (1)$$

where α, h, ν, B, and E_g represent absorption coefficients, the Planck constant, light frequency, a proportionality constant,

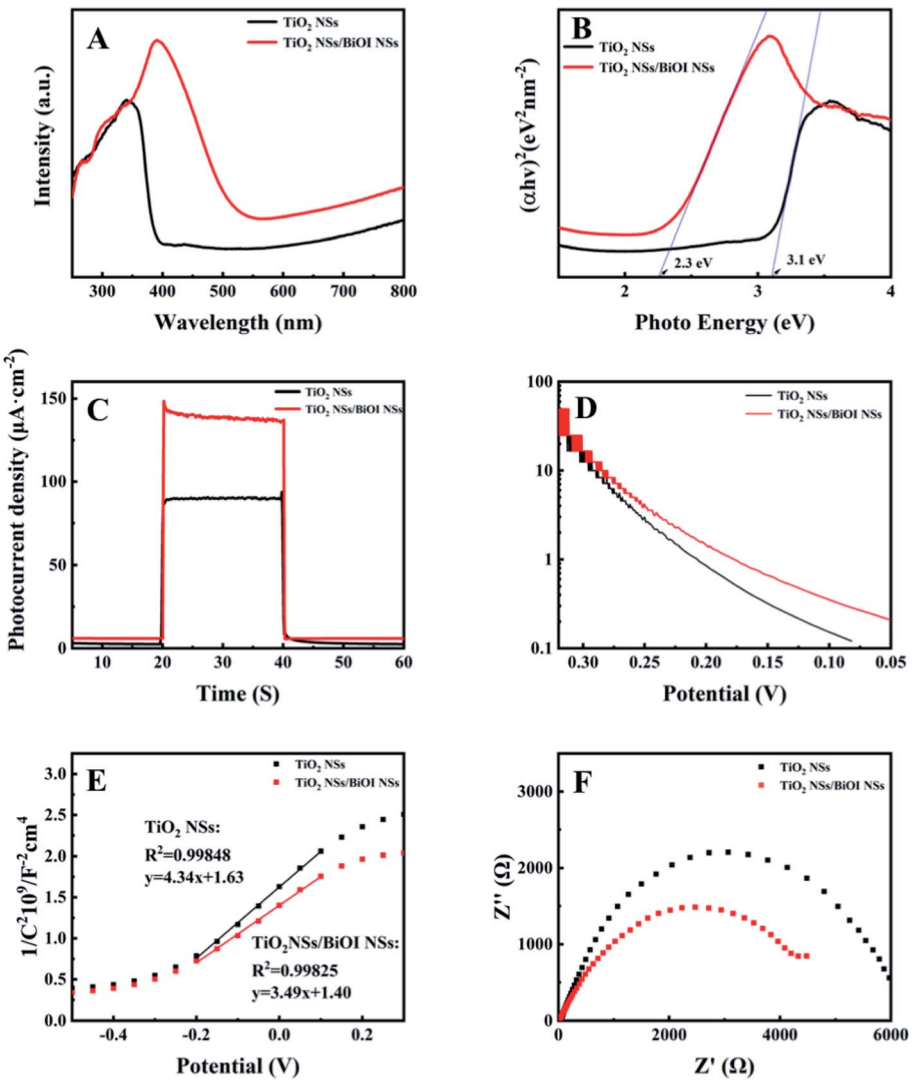

Fig. 4 (A) UV-vis diffuse reflectance spectra of TiO_2 NSs (black curve) and TiO_2 NSs/BiOI NSs (red curve). (B) Plots of $(F(R)h\nu)^{1/2}$ *versus* E (eV). (C) Photocurrent responses of TiO_2 NSs and TiO_2 NSs/BiOI NSs electrodes. (D) Electronic lifetimes in 0.1 M PBS (pH = 7.4). (E) Mott–Schottky plots. (F) EIS Nyquist plots.

and the energy band gap, respectively. TiO_2 and BiOI are indirect semiconductors, so the value of n is 1/2. The data were brought in, and the band gap values of TiO_2 NSs and TiO_2 NSs/BiOI NSs were 3.1 and 2.3 eV, respectively, as shown in Fig. 4B.

Fig. 4C shows the photoelectrical response of TiO_2 NSs and TiO_2 NS/BiOI NS electrodes under simulated sunlight irradiation. The electrode was significantly improved after the BiOI NSs were modified. To explore the PEC performance of the electrode further, a three-electrode system was constructed to detect the intrinsic electronic characteristics of the electrode, where the TiO_2NS/BiOI NS electrode was the working electrode, a Pt electrode was the counter electrode, and an Ag/AgCl electrode was the reference electrode (saturated KCl).

The electrode generated a photovoltage as photogenerated electron–hole pairs accumulated on the cathode and anode under illumination.[22] When the light was canceled, the photogenerated holes collected on the anode and the photogenerated electrons collected on the cathode quickly recombined, and then the open circuit potential was recorded. The lifetime of the photogenerated carriers could be calculated with formula (2).[23]

$$\tau = \frac{k_B T}{e}\left(\frac{dV_\alpha}{dt}\right)^{-1}, \quad (2)$$

where τ is the electron lifetime; V_α is the open-circuit voltage at time t; k_B, e, and T are the Boltzmann constant, absolute temperature, and charge of a single electron, respectively. The electron lifetime of the corresponding samples could be calculated from known, measured data, and the result is shown in Fig. 4D. Clearly, the carrier lifetime of the TiO_2 NS/BiOI NS electrode is greater than that of TiO_2 NSs. Consequently, by forming a heterojunction with BiOI NSs, the carrier lifetime of the TiO_2 NS electrode is significantly prolonged, and the separation of carriers is promoted.

Formula (3)[24] was used to calculate capacitance, and the carrier density (N_D) could be obtained through its conversion form.

$$\frac{1}{C^2} = \frac{2}{N_D e \varepsilon_0 \varepsilon}\left[(U_S - U_{FB}) - \frac{k_B T}{e}\right], \quad (3)$$

where C is the space charge capacitance; e is the element charge value; ε_0 and ε are vacuum permittivity and relative permittivity, respectively; U_S and U_{FB} are the applied potential and Fermi energy in the semiconductor, respectively; k_B is the Boltzmann constant; T is the temperature.

After conversion, the formula for the calculation of N_D was as follows:

$$N_D = -\left(\frac{2}{e\varepsilon_0\varepsilon}\right)\left(\frac{d\left(\frac{1}{C^2}\right)}{d(U_S)}\right)^{-1}, \quad (4)$$

where N_D is inversely proportional to the first derivative of $1/C^2$. Hence, the slope value linearly fitted by the samples could be

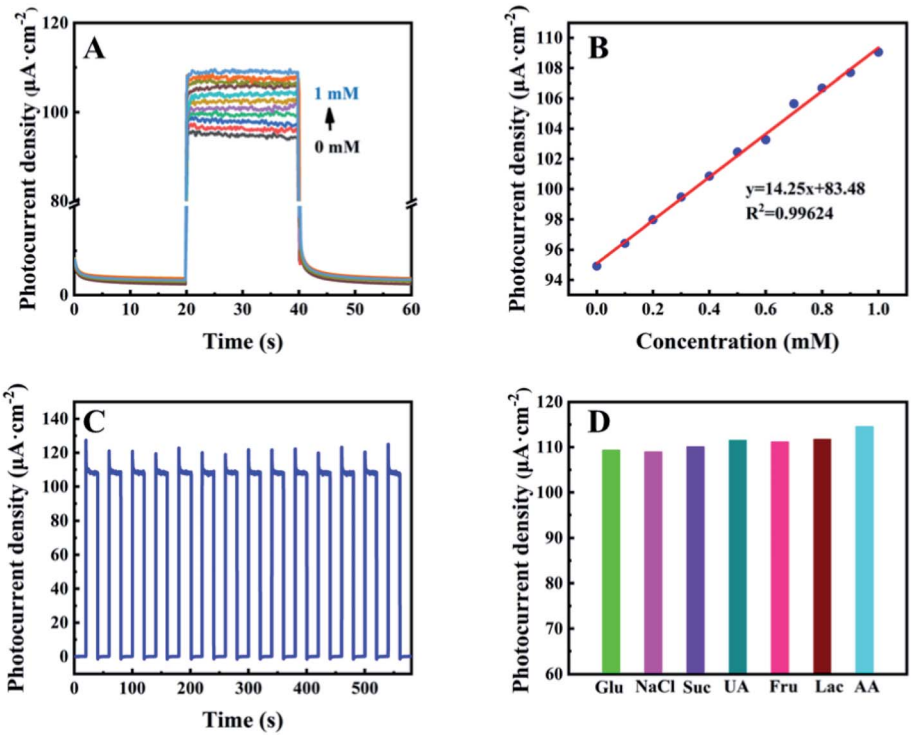

Fig. 5 (A) Photocurrent responses of the TiO_2 NSs/BiOI NSs/GOx biosensor toward different concentrations of glucose from 0 mM to 1 mM in 0.1 M PBS (pH 7.4) electrolyte. (B) Linear calibration between glucose concentration and photocurrent density. (C) Stability under light conditions in the presence of 1 mM glucose. (D) Detection of the anti-interference performance of the electrode. The experiments were conducted in 0.1 M PBS (pH 7.4) at concentrations of 0.1 mM NaCl, sucrose (Suc), uric acid (UA), fructose (Fru), lactose (Lac), and ascorbic acid (AA) in the presence of 1 mM glucose.

Table 1 A comparison of the analytical characteristics of this sensor and other sensors used to detect glucose

GOx PEC biosensor	Linear range (mM)	Sensitivity ($\mu A\ mM^{-1}\ cm^{-2}$)	Ref.
GOx/SnS_2/Nafion/GCE	0.025–1.10	7.6	25
Nafion/GOx/Ag-Pdop@CNT/GCE	0.050–1.10	3.1	26
GCE/GOx/Nafion/Br/TNT–AuNP	0.01–1.2	5.1	27
GOx/CNx–MWCNT/GCE	0.02–1.02	13	28
Nafion/GOx/PANI@GO/GCE	0.07–1.1	10.81	29
TiO_2 NSs/BiOI NSs/GOx	0.01–1.00	14.25	This work

used to compare the carrier density qualitatively. The measured data were brought into the formula and a linear fit applied, and the result is shown in Fig. 4E. The carrier density of the TiO_2 NS/BiOI NS electrode improved compared with the TiO_2 NS electrode. Moreover, the positive slope of the MS curve indicates that the prepared TiO_2 NS/BiOI NS electrode has n-type characteristics.

Electrochemical impedance spectroscopy (EIS) was performed to study the interface characteristics of the photoelectrodes and the dynamics of charge transfer. Fig. 4F shows that in the same frequency range, the prepared TiO_2 NS/BiOI NS composite electrode has a smaller radius, indicating that it has higher conductivity and photoelectric conversion efficiency.

Based on the good optoelectronic properties of the electrodes, the electrodes were constructed and tested for PEC enzymatic sensing under simulated sunlight and visible light (420 nm). Fig. 5A shows the glucose concentration gradient measured on the prepared TiO_2 NS/BiOI NS/GOx electrode. As the glucose concentration increased, the value of the photocurrent also rose, indicating a sensitive reaction to glucose concentration. The relationship between the glucose concentration and photocurrent density in simulated sunlight satisfies the equation J (photocurrent density) ($\mu A\ cm^{-2}$) = 14.25[Glu] (mM) + 83.48 (mM), and the statistically significant correlation coefficient is 0.99624 (Fig. 5B). Thus, the sensitivity of the biosensor under simulated sunlight is 14.25 $\mu A\ mM^{-1}\ cm^{-2}$, the detection range for glucose is 0–1 mM, and the LOD (3S/N) is 0.01 mM. Fig. S3† shows that in the 0–0.1 mM range of glucose, the sensitivity of detection under visible light is 0.571 $\mu A\ mM^{-1}\ cm^{-2}$.

The stability of the TiO_2 NSs/BiOI NSs/GOx electrode was tested at 1 mM glucose by brief illumination for 600 s. Fig. 5C displays that the examined outcome shows that the photocurrent of the TiO_2 NSs/BiOI NSs/GOx electrode absolutely does not change with time.

Specificity and selectivity are important indices to judge the capability of a sensor. Possible coexisting and common molecules in the serum were selected as interfering substances, such as sucrose (Suc), fructose (Fru), uric acid (UA), ascorbic acid (AA), lactose (Lac), and NaCl to test the TiO_2 NSs/BiOI NSs/GOx biosensor. The results are shown in Fig. 5D. All kinds of interferers show no significant effect, indicating that the TiO_2 NSs/BiOI NSs/GOx biosensor has excellent anti-interference performance due to the selective catalysis of GOx fixed on TiO_2 NSs/BiOI NSs.

The performance of the PEC biosensor designed in this work was compared with some published glucose sensors, as listed in Table 1. The performance of the biosensor in this work on the two parameters of sensitivity and detection range is acceptable.

The satisfactory behavior of the PEC biosensor is attributed to the excellent photogenerated carrier separation mechanism shown in Scheme 2.

The TiO_2 NSs prepared in this paper expose a large proportion of (001) facets. The (101) and (001) facets of TiO_2 are identified as

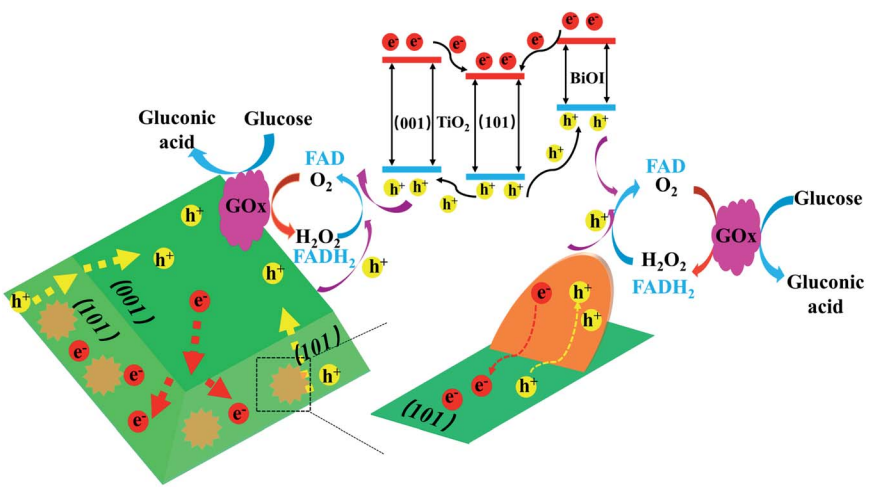

Scheme 2 The manufacturing of the TiO_2 NS/BiOI NS/GOx biosensor and the PEC-sensing strategy for glucose detection.

electron-rich and hole-rich planes,[30] respectively. The photogenerated electrons generated on the (001) facets would migrate autonomously to the (101) facets. On the NSs, the (101) and (001) crystal facets were adjacent to each other and should have equal Fermi levels, so the two parts could form crystal facet heterojunctions,[31,32] which gives the TiO_2 NS single crystal material better photoelectric self-separation performance.[33,34] When BiOI NSs form a p–n heterogeneous structure with TiO_2 NSs, the Fermi level of BiOI and TiO_2 shifts until a new equilibrium is reached.[35,36] Under irradiation, the photogenerated electrons from TiO_2 and BiOI are gathered to TiO_2 (101) and exported through the FTO substrates to generate electrical signals. The photogenerated holes are transferred to TiO_2 (001) and BiOI to participate in the enzymatic reaction that oxidizes H_2O_2 to O_2. Thus, the TiO_2 NS/BiOI NS electrode could effectively promote the separation of the photogenerated electron–hole pairs and improve the PEC performance, which is crucial for achieving the outstanding analytical performance of the sensing platform.

4. Conclusions

A TiO_2 NS/BiOI NS photoelectrode was manufactured *via* hydrothermal and solvothermal methods on an FTO substrate, where the anatase TiO_2 film had a high percentage of (001) facets and BiOI NSs selectively grew on the TiO_2 (101) facets. Coupling with BiOI NSs broadened the absorption in the visible light region, extended the carrier lifetime, increased the photocurrent density, and significantly enhanced the PEC performance. The prepared TiO_2 NSs/BiOI NSs/GOx glucose biosensor under simulated sunlight achieved satisfactory results: the sensitivity was 14.25 $\mu A\ mM^{-1}\ cm^{-2}$, the linear measurement range was 0–1 mM, and the LOD (3S/N) was 0.01 mM in PBS buffer at pH 7.4. In addition, the mechanism for the efficient separation of photogenerated carriers based on the crystal facet heterojunctions introduced in this paper could be used as a reference for the detection of other substances, such as nucleic acids, oxidases, and proteins.

Conflicts of interest

The authors declare no competing financial interests.

Acknowledgements

We gratefully acknowledge project support from Hainan Province Clinical Medical Center, the Finance Science and Technology Project of Hainan Province (ZDYF2021SHFZ068, and ZDKJ2021029), the National Natural Science Foundation of China (nos. 51862006), CAMS Innovation Fund for Medical Sciences (no. 2019-I2M-5-023), and Key Laboratory Open Project Fund of Emergency and Trauma of Ministry of Education (no. KLET-202008, 201910).

References

1 T. Hou, L. F. Zhang, X. Z. Sun and F. Li, Biphasic photoelectrochemical sensing strategy based on in situ formation of CdS quantum dots for highly sensitive detection of acetylcholinesterase activity and inhibition, *Biosens. Bioelectron.*, 2016, **75**, 359–364.

2 T. Hou, N. N. Xu, W. X. Wang, L. Ge and F. Li, Truly Immobilization-Free Diffusivity-Mediated Photoelectrochemical Biosensing Strategy for Facile and Highly Sensitive MicroRNA Assay, *Anal. Chem.*, 2018, **90**(15), 9591–9597.

3 S. Feng, J. Yang, H. Zhu, M. Liu, J. Zhang, J. Wu and J. Wan, Synthesis of Single Crystalline Anatase TiO_2 (001) Tetragonal Nanosheet-Array Films on Fluorine-Doped Tin Oxide Substrate, *J. Am. Ceram. Soc.*, 2011, **94**(2), 310–315.

4 W. K. Yang, W. Xu, Y. D. Wang, D. L. Chen, X. H. Wang, Y. Cao, Q. Wu, J. C. Tu and C. Zhen, Photoelectrochemical Glucose Biosensor Based on the Heterogeneous Facets of Nanocrystalline TiO_2/Au/Glucose Oxidase Films, *ACS Appl. Nano Mater.*, 2020, **3**(3), 2723–2732.

5 M. Shah, K. Zhang, A. R. Park, K. S. Kim, N. G. Park, J. H. Park and P. J. Yoo, Single-step solvothermal synthesis of mesoporous Ag-TiO_2-reduced graphene oxide ternary composites with enhanced photocatalytic activity, *Nanoscale*, 2013, **5**(11), 5093–5101.

6 G. C. Fan, M. Zhao, H. Zhu, J. J. Shi, J. R. Zhang and J. J. Zhu, Signal-on Photoelectrochemical Aptasensor for Adenosine Triphosphate Detection Based on Sensitization Effect of CdS:Mn@Ru(bpy)(2)(dcbpy) Nanocomposites, *J. Phys. Chem. C*, 2016, **120**(29), 15657–15665.

7 S. Cakar and M. Özacar, The effect of iron complexes of quercetin on dye-sensitized solar cell efficiency, *J. Photochem. Photobiol., A*, 2017, **346**, 512–522.

8 X. Liu, R. Yan, J. Zhu, X. Huo and X. Wang, Development of a photoelectrochemical lactic dehydrogenase biosensor using multi-wall carbon nanotube-TiO_2 nanoparticle composite as coenzyme regeneration tool, *Electrochim. Acta*, 2015, **173**, 260–267.

9 M. Arumugam, Y. Yu, H. J. Jung, S. Yeon, H. Lee, J. Theerthagiri, S. J. Lee and M. Y. Choi, Solvent-mediated synthesis of BiOI with a tunable surface structure for effective visible light active photocatalytic removal of Cr(VI) from wastewater, *Environ. Res.*, 2021, **197**, 111080.

10 W. W. Zhao, S. Shan, Z. Y. Ma, L. N. Wan, J. J. Xu and H. Y. Chen, Acetylcholine esterase antibodies on BiOI nanoflakes/TiO_2 nanoparticles electrode: a case of application for general photoelectrochemical enzymatic analysis, *Anal. Chem.*, 2013, **85**(24), 11686–11690.

11 L. F. Fan, G. F. Liang, C. Y. Zhang, L. Fan, W. J. Yan, Y. J. Guo, S. M. Shuang, Y. P. Bi, F. Li and C. Dong, Visible-light-driven photoelectrochemical sensing platform based on BiOI nanoflowers/TiO_2 nanotubes for detection of atrazine in environmental samples, *J. Hazard. Mater.*, 2021, **409**, 124894.

12 Z. Liu, W. C. Xu, J. Z. Fang, X. X. Xu, S. X. Wu, X. M. Zhu and Z. H. Chen, Decoration of BiOI quantum size nanoparticles with reduced graphene oxide in enhanced visible-light-driven photocatalytic studies, *Appl. Surf. Sci.*, 2012, **259**, 441–447.

13 X. Zhang, L. Z. Zhang, T. F. Xie and D. J. Wang, Low-Temperature Synthesis and High Visible-Light-Induced

Photocatalytic Activity of BiOI/TiO_2 Heterostructures, *J. Phys. Chem. C*, 2009, **113**(17), 7371–7378.

14 C. X. Liao, Z. J. Ma, G. P. Dong and J. R. Qiu, BiOI nanosheets decorated TiO_2 nanofiber: Tailoring water purification performance of photocatalyst in structural and photo-responsivity aspects, *Appl. Surf. Sci.*, 2014, **314**, 481–489.

15 M. J. Islam, D. A. Reddy, J. Choi and T. K. Kim, Surface oxygen vacancy assisted electron transfer and shuttling for enhanced photocatalytic activity of a Z-scheme CeO_2-AgI nanocomposite, *RSC Adv.*, 2016, **6**(23), 19341–19350.

16 G. P. Dai, J. G. Yu and G. Liu, Synthesis and Enhanced Visible-Light Photoelectrocatalytic Activity of p–n Junction BiOI/TiO_2 Nanotube Arrays, *J. Phys. Chem. C*, 2011, **115**(15), 7339–7346.

17 X. S. Zhou, B. Jin, L. D. Li, F. Peng, H. J. Wang, H. Yu and Y. P. Fang, A carbon nitride/TiO_2 nanotube array heterojunction visible-light photocatalyst: synthesis, characterization, and photoelectrochemical properties, *J. Mater. Chem.*, 2012, **22**(34), 17900–17905.

18 T. Butburee, Y. Bai, H. Wang, Z. Wang, G. Liu, J. Zou, P. Khemthong, G. Qing Max Lu and L. Wang, 2D Porous TiO_2 Single-Crystalline Nanostructure Demonstrating High Photo-Electrochemical Water Splitting Performance, *Adv. Mater.*, 2018, **30**, 1705666.

19 H. G. Yang, C. H. Sun, S. Z. Qiao, J. Zou, G. Liu, S. C. Smith, H. M. Cheng and G. Q. Lu, Anatase TiO_2 single crystals with a large percentage of reactive facets, *Nature*, 2008, **453**(7195), 638–641.

20 J. X. Ma, M. M. Zhang, W. Su, B. Q. Wu, Z. Yang, X. H. Wang, B. Qiao, H. Pei, J. C. Tu, D. L. Chen and Q. Wu, Photoelectrochemical Enzyme Biosensor Based on TiO_2 Nanorod/TiO_2 Quantum Dot/Polydopamine/Glucose Oxidase Composites with Strong Visible-Light Response, *Langmuir*, 2022, **38**(2), 751–761.

21 L. P. Zhu, L. L. Wang, N. C. Bing, C. Huang, L. J. Wang and G. H. Liao, Porous Fluorine-Doped gamma-Fe_2O_3 Hollow Spheres: Synthesis, Growth Mechanism, and Their Application in Photocatalysis, *ACS Appl. Mater. Interfaces*, 2013, **5**(23), 12478–12487.

22 B. D. Yan, X. R. Zhao, D. L. Chen, Y. Cao, C. Z. Lv, J. C. Tu, X. H. Wang and Q. Wu, Enhanced photoelectrochemical biosensing performance for Au nanoparticle-polyaniline-TiO_2 heterojunction composites, *RSC Adv.*, 2020, **10**(72), 43985–43993.

23 B. H. Meekins and P. V. Kamat, Got TiO_2 Nanotubes? Lithium Ion Intercalation Can Boost Their Photoelectrochemical Performance, *ACS Nano*, 2009, **3**(11), 3437–3446.

24 Y. M. Xin, Z. Z. Li and Z. H. Zhang, Photoelectrochemical aptasensor for the sensitive and selective detection of kanamycin based on Au nanoparticle functionalized self-doped TiO_2 nanotube arrays, *Chem. Commun.*, 2015, **51**(85), 15498–15501.

25 Z. Yang, Y. Ren, Y. Zhang, J. Li, H. Li, X. Hu and Q. Xu, Nanoflake-like SnS_2 matrix for glucose biosensing based on direct electrochemistry of glucose oxidase, *Biosens. Bioelectron.*, 2011, **26**(11), 4337–4341.

26 Y. Wang, L. Liu, M. Li, S. Xu and F. Gao, Multifunctional carbon nanotubes for direct electrochemistry of glucose oxidase and glucose bioassay, *Biosens. Bioelectron.*, 2011, **30**(1), 107–111.

27 J. Zhu, K. Y. Wong Danny, R. Zhao and J. Zhang, Enhancing Direct Electron Transfer of Glucose Oxidase Using a Gold Nanoparticle Vertical Bar Titanate Nanotube Nanocomposite on a Biosensor, *Electrochim. Acta*, 2015, **163**, 64–70.

28 S. Deng, G. Jian, J. Lei, Z. Hu, H. Ju, S. Deng, et al., A glucose biosensor based on direct electrochemistry of glucose oxidase immobilized on nitrogen-doped carbon nanotubes, *Biosens. Bioelectron.*, 2009, **25**(2), 373–377.

29 Z. P. Kang, K. L. Jiao, X. P. Xu, R. Y. Peng, S. Q. Jiao and Z. Q. Hu, Graphene oxide-supported carbon nanofiber-like network derived from polyaniline: A novel composite for enhanced glucose oxidase bioelectrode performance, *Biosens. Bioelectron.*, 2017, **96**, 367–372.

30 S. Selcuk and A. Selloni, Facet-dependent trapping and dynamics of excess electrons at anatase TiO_2 surfaces and aqueous interfaces, *Nat. Mater.*, 2016, **15**(10), 1107–+.

31 J. Pan, G. Liu, G. M. Lu and H. M. Cheng, On the True Photoreactivity Order of {001}, {010}, and {101} Facets of Anatase TiO_2 Crystals, *Angew. Chem., Int. Ed.*, 2011, **50**(9), 2133–2137.

32 W. K. Wang, J. J. Chen, Z. Z. Lou, S. Kim, M. Fujitsuka, H. Q. Yu and T. Majima, Single-molecule and particle probing crystal edge/corner as highly efficient photocatalytic sites on a single TiO_2 particle, *Proc. Natl. Acad. Sci. U. S. A.*, 2019, **116**(38), 18827–18833.

33 T. Tachikawa, S. Yamashita and T. Majima, Evidence for Crystal-Face-Dependent TiO_2 Photocatalysis from Single-Molecule Imaging and Kinetic Analysis, *J. Am. Chem. Soc.*, 2011, **133**(18), 7197–7204.

34 J. G. Yu, J. X. Low, W. Xiao, P. Zhou and M. Jaroniec, Enhanced Photocatalytic CO_2-Reduction Activity of Anatase TiO_2 by Coexposed {001} and {101} Facets, *J. Am. Chem. Soc.*, 2014, **136**(25), 8839–8842.

35 S. Q. Luo, C. Tang, Z. H. Huang, C. Liu, J. W. Chen and M. H. Fang, Effect of different Bi/Ti molar ratios on visible-light photocatalytic activity of BiOI/TiO_2 heterostructured nanofibers, *Ceram. Int.*, 2016, **42**(14), 15780–15786.

36 Y. Zhao, X. Huang, X. Tan, T. Yu, X. L. Li, L. B. Yang and S. C. Wang, Fabrication of BiOBr nanosheets@TiO_2 nanobelts p–n junction photocatalysts for enhanced visible-light activity, *Appl. Surf. Sci.*, 2016, **365**, 209–217.